Hindawi
Geofluids
Volume 2022, Article ID 4260540, 23 pages
https://doi.org/10.1155/2022/4260540

Research Article

Analysis of Effects of Rough Strip Energy Dissipator on Hydraulic Property of Bend Flow

Honghong Zhang,[1,2] **Zhenwei Mu**,[1,2] **Fan Fan**,[1,2] **and Fanqi Li**[3]

[1]*College of Water Conservancy and Civil Engineering, Xinjiang Agricultural University, Urumqi, China*
[2]*Xinjiang Key Laboratory of Hydraulic Engineering Security and Water Disasters Prevention, Urumqi, China*
[3]*Jiufan Engineering Design Consulting Co., Ltd., Hefei, China*

Correspondence should be addressed to Zhenwei Mu; muzhenwei@xjau.edu.cn

Received 22 June 2022; Revised 17 August 2022; Accepted 1 September 2022; Published 7 October 2022

Academic Editor: Zhiyuan Wang

Installing rough strip energy dissipators (R-SEDs) at the bottom of curved spillways can facilitate energy dissipation and flow stabilization. In this study, the effects of R-SEDs set at the bottom of a 60° bend in a spillway were examined. This spillway had a large width-to-depth ratio ($B/H > 5$). Based on physical model tests, the distribution of hydraulic properties of the spillway under different runs was studied and analyzed. The results show that the R-SEDs effectively improved the flow pattern in the bend. The R-SEDs reduced the average dimensionless flow velocity by about 37.9% by increasing the roughness at the bottom of the bend. The energy dissipation rate of the R-SED decreased with an increase in discharge flow rate and ranged between 30% and 50%. These indicate that it is feasible to apply the R-SEDs to 60° bends of spillways with a large width-to-depth ratio at low-flow runs (the tested discharge flow rate = 15 L/s). These results will provide a theoretical basis for the R-SED design of similar curved spillways.

1. Introduction

As an important component of a dam, the spillway plays a crucial role in ensuring its engineering safety and expected benefits [1–4]. A spillway usually consists of a control structure, a discharge channel, a terminal structure, and an inlet or outlet channel [2, 4, 5]. Particularly, the discharge flow in a discharge channel has a high velocity and energy. Thus, energy dissipators are commonly required in the discharge channel to dissipate excess energy and thus reduce the scouring of downstream buildings and channels by the discharge flow [2, 5]. Spillways are generally divided into straight and curved types based on the arrangement of discharge channels. Due to their better hydraulic conditions and higher practicality, straight spillways are commonly adopted in most projects. However, the application of straight spillways is constrained by topographic and geological conditions, engineering characteristics, construction conditions, and economic indicators [1, 6, 7]. Some curved spillways are also employed worldwide. For example, the curved spillways in China include the Lubuge Hydropower Station spillway in Yunnan, the Yin'ejike 635 Reservoir spillway in Xinjiang, and the Taihu Reservoir spillway in Zhejiang. The water flow through a bend (i.e., the bend flow) is different from the straight flow. Due to the combined effect of inertial centrifugal forces and bend slope, uneven distribution of water depth at both banks, uneven cross-sectional velocity distribution, and secondary flows may occur in curved spillways [4, 7, 8]. These complex flow patterns lead to sediment movement, riverbed evolution, and channel deformation [9].

In 1876, Thompson [10] first proposed the problem of bend circulation based on experimental research. Since then, most researchers have investigated the basic characteristics of bend flow, such as water depth distribution [4, 11–14], flow velocity distribution [6, 12–22], and secondary flow [6, 13, 14, 16, 18, 20, 23–28]. With the knowledge of the characteristics of bend flow, some researchers have improved bend flow patterns by considering different engineering measures, such as guide walls [4], permeable spur

dikes [7], vanes [15, 29], and ripraps [30]. However, studies on engineering measures to improve bend flow patterns and their application to spillways with large width (B)-to-depth (H) ratios ($B/H > 5$) are still insufficient. Therefore, in this study, rough strip energy dissipators (R-SEDs) were added to the 60° bend of a spillway with a large B/H. The R-SEDs are simple in shape and easy to construct and can effectively mitigate adverse hydraulic phenomena of curved spillways. Thus, the R-SEDs will facilitate the safety and stable operation of curved spillways and continuous water use downstream of the building (e.g., industrial and irrigation water).

This research was based on the hydraulic model test of the curved spillway of the Yin'ejike 635 Reservoir in Xinjiang, China (the geometric scale was 1 : 50). At a discharge flow rate of 800 m^3/s, the water depth and flow velocity at the concave and convex banks were significantly different, and the bend flow was turbulent. To tackle these flow issues, R-SEDs have been arranged at the bottom of the bend in our previous research [31], showing high effectiveness in energy dissipation and diversion of bend flow. Since then, the R-SEDs have been increasingly investigated, while studies on R-SEDs are still insufficient. Li [31] mainly analyzed the effects of R-SEDs on water depth and flow velocity in the bend based on a hydraulic model of the Yin'ejike 635 Reservoir spillway. Thus, the analysis of the changes in the hydraulic properties of bend flow after the R-SEDs were installed was not comprehensive. Fan et al. [32] mainly analyzed the energy dissipation rate of the R-SEDs but did not systematically analyze their hydraulic properties. Therefore, in this paper, multiple factors affecting water flow patterns and hydraulic properties of the R-SEDs applied to the 60° bend of the spillway with a large B/H were investigated using hydrodynamic theory and physical model tests. This study is anticipated to improve the practicability and universality of the R-SEDs and provide some theoretical basis and support for similar projects.

2. Experiments

2.1. Physical Model. The test was completed in the curved spillway flume of the Xinjiang Key Laboratory of Water Conservancy Engineering Safety and Water Disaster Prevention, China. Laboratory studies are typically conducted using geometrically similar models [5]. The physical model in this study was designed according to the gravity similarity criterion (Froude similarity criterion). The Froude number and Reynolds number at each test run are shown in Table 1. The test system included a model test section and a water circulation system. The model test section consisted of a straight inlet section, a 60° bend and a straight outlet section, with a slope (i) of 0.025 along the spillway. The parameters of the test section were arranged as follows: the cross-section of the flume was a regular rectangle with a width $B = 0.5$ m; the length of the straight inlet section, $L_1 = 1.0$ m; the total arc length of the 60° bend, $S = 0.79$ m; the centerline radius, $R_0 = 0.75$ m; the inner diameter, $R_1 = 0.5$ m; the outer diameter, $R_2 = 1.0$ m; and the length of the straight outlet section, $L_2 = 2.0$ m. The water circulation system consisted of a water pump, a rectangular water storage tank, a flow measuring weir, an underground reservoir, and underground water pipes. There were 27 data measurement cross-sections along the model test section, and the measurement points #0-#10 were established in sequence from the convex bank to the concave bank for each section. The test setup and section settings are illustrated in Figure 1, where s and n represent the transverse and longitudinal flow directions, respectively.

Table 1: Parameter settings of test runs.

Run	h_1/h_2 (cm)	θ (°)	ΔL (cm)	Q (L/s)	Number of R-SEDs	Froude number	Reynolds number
1	1.0/0.5	20	17	15	7	1.84	29992.77
2	1.0/0.5	20	17	25	7	1.78	47752.44
3	1.0/0.5	20	17	35	7	1.66	63927.14
4	1.5/0.75	20	17	15	7	1.90	30056.19
5	1.5/0.75	20	17	25	7	1.77	47724.32
6	1.5/0.75	20	17	35	7	1.73	64220.43
7	2.0/1.0	20	17	15	7	1.72	29840.67
8	2.0/1.0	20	17	25	7	1.74	47649.00
9	2.0/1.0	20	17	35	7	1.58	63520.25
10	1.5/0.75	20	9	15	12	1.03	28543.47
11	1.5/0.75	20	9	25	12	1.14	45457.34
12	1.5/0.75	20	9	35	12	1.19	61143.80
13	1.5/0.75	20	25	15	5	1.17	28896.12
14	1.5/0.75	20	25	25	5	1.25	45929.21
15	1.5/0.75	20	25	35	5	1.26	61638.58
16	1.5/0.75	0	17	15	7	1.02	28505.60
17	1.5/0.75	0	17	25	7	1.10	45222.36
18	1.5/0.75	0	17	35	7	1.28	61786.98
19	1.5/0.75	40	17	15	7	1.91	30067.93
20	1.5/0.75	40	17	25	7	1.71	47568.04
21	1.5/0.75	40	17	35	7	1.70	64103.94

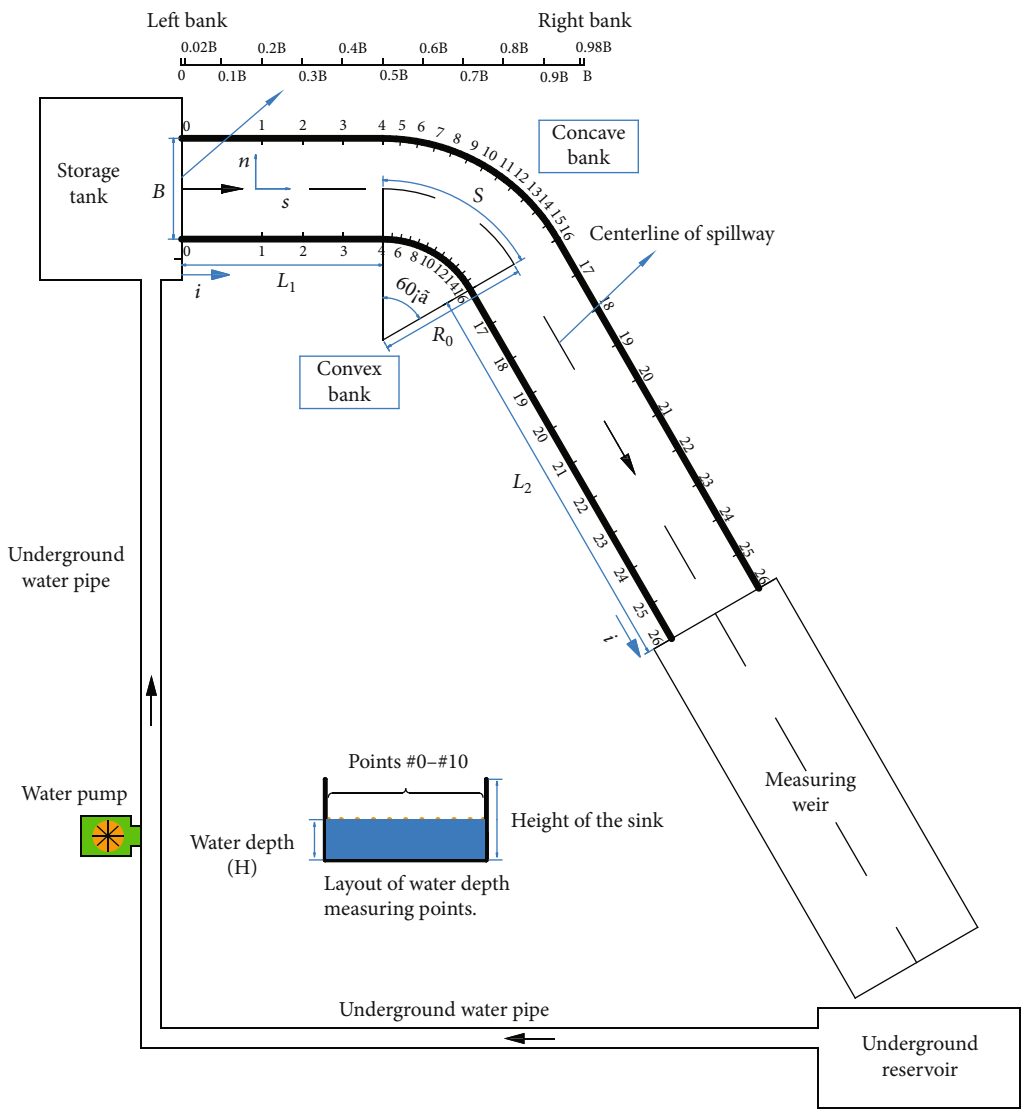

(a)

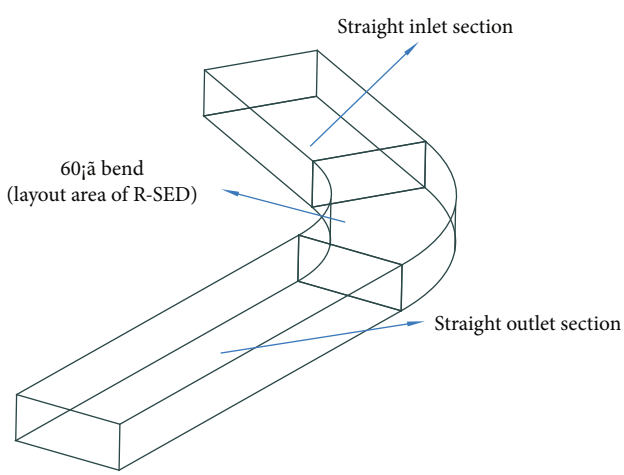

(b)

Figure 1: Continued.

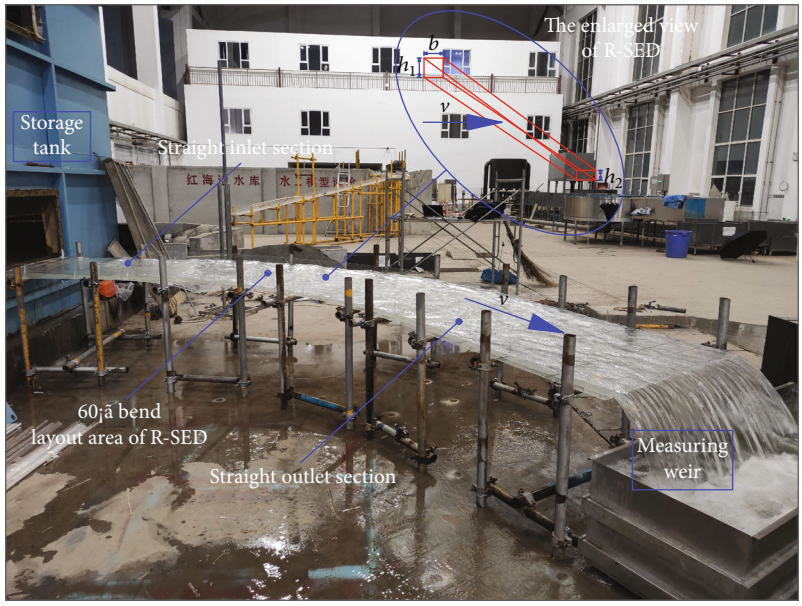

(c)

Figure 1: (a) Plane layout of experimental setup and setting of measurement cross-sections; (b) three-dimensional structure of the spillway; (c) photo of the physical model.

The R-SEDs were located at the 60° bend of the spillway. Each R-SED extended continuously from the concave bank to the convex bank and was close to the bottom of the bend. Due to the different heights of the R-SEDs at the concave and convex banks, the longitudinal cross-section of the R-SEDs was trapezoidal. The arrangement parameters of the R-SEDs included the height, angle, and spacing. h_1 and h_2 denote the height of the R-SED at the concave and convex banks ($h_1 > h_2$), respectively, and thus, the height of the R-SED was expressed as h_1/h_2. The cross-sections of the R-SEDs (both concave and convex banks) were all regular rectangles. The angle of an R-SED, θ, refers to the angle between the R-SED and the direction of the longitudinal axis of the flow channel. The spacing of R-SEDs, ΔL, refers to the arc distance between the centerlines of adjacent R-SEDs. b is the R-SED thickness, and l is the longitudinal length of each R-SED. The arrangement parameters and shape of the R-SEDs are shown in Figure 2.

2.2. Setup Runs. Different arrangement parameters of the R-SEDs resulted in different layout types, which may have energy dissipation effects. Based on the hydraulic model test results of the Yin'ejike 635 Reservoir spillway incorporating the R-SEDs [31], three typical heights (h_1/h_2), angles (θ), spacings (ΔL), and discharge flow rates (Q) were selected to form 21 test runs. The parameter settings of the 21 test runs are shown in Table 1. The first and last R-SEDs were arranged at the inlet cross-section (#4) and the outlet cross-section (#16) of the bend, respectively. In each run, the spacing of the R-SEDs determined the number of R-SEDs. To avoid duplicated parameter analysis, the number of R-SEDs was not considered as a separate parameter. Table 1 shows the number of R-SEDs in the 21 runs.

2.3. Instrumentation. The water depths and flow velocities in the 27 cross-sections along the spillway (Figure 1(a)) were measured, and 11 measurement points were arranged for each cross-section and labeled as measurement points #0-#10. Points #0 and #10 were the convex and concave bank measurement points, respectively. The water depth was measured using needle water-level gauges with an accuracy of 0.1 mm. Considering the wide shallow model flow and the low flow velocity, the flow velocity was measured using a Pitot tube with an accuracy of 0.1 mm. The discharge flow rate was measured using a thin-walled right triangular (90°) weir. The shape of the weir mouth is shown in Figure 3. The discharge flow rate is expressed as

$$Q = C_0 H_1^{5/2}, \tag{1}$$

where Q is the discharge flow rate (m^3/s), H_1 is the water depth above the weir (m), and C_0 is the flow coefficient of the thin-walled triangular weir, which is related to the opening angle. C_0 is calculated through

$$C_0 = 1.354 + \frac{0.004}{H_1} + \left(0.14 + \frac{0.2}{\sqrt{P_1}}\right)\left(\frac{H_1}{B_1} - 0.09\right)^2, \tag{2}$$

where P_1 is the height of the weir (m) and B_1 is the width of the diversion channel upstream of the weir (m).

3. Results and Discussion

3.1. Water Surface Structure. Our previous study (a model test was designed according to the gravity similarity criterion and had a geometric scale of 1 : 50) has shown that the R-SEDs are more suitable for the spillways with a low

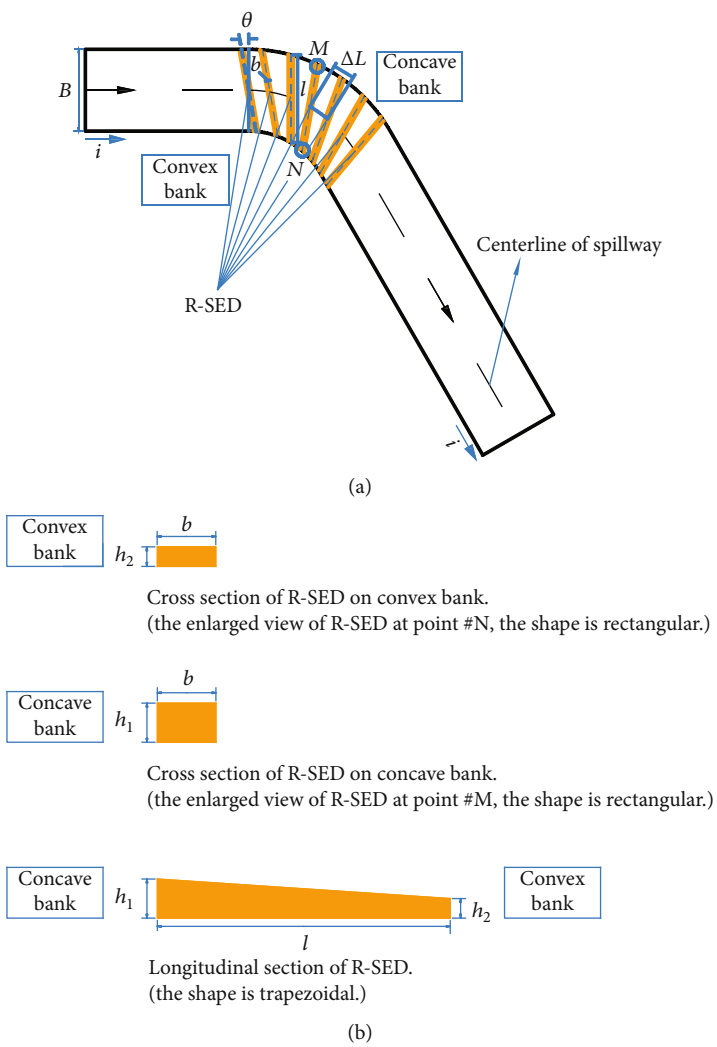

Figure 2: (a) Schematic diagram of R-SEDs arrangement in the curved spillway and related parameters; (b) schematic diagram of R-SED structure.

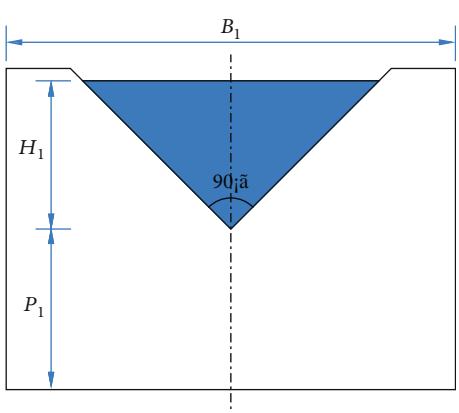

Figure 3: Illustration of the thin-walled right triangular weir mouth.

discharge flow rate (the tested flow $Q \leq 20$ L/s) but a high B/H ($B/H > 5$). At a low discharge flow rate, the inclusion of R-SEDs in the spillway bend reduced the influence of centrifugal force in the bend on the water surface. The phenomenon of "water depth increasing at the concave bank but decreasing at the convex bank" did not occur, and the water surface tended to be steady [32]. Seven runs with a low flow rate (15 L/s) (Runs 1, 4, 7, 10, 13, 16, and 19) were selected to compare with the run without R-SEDs in terms of water surface structures. Figures 4(a)–4(h) show the water surface structures in the run without R-SEDs and the seven selected runs. Figure 4(a) shows that without R-SEDs at the bottom of the bend, the flow entering the bend through the straight inlet section was affected by centrifugal forces. The water depth of the bend flow increased at the concave bank but decreased at the convex bank. The water distributions of Cross-sections #5-#16 were uneven. The flow out of the bend was supported by the side wall and formed a folded flow in the straight section of the downstream outlet. The flow distributions of Cross-sections #17-#26 were relatively uneven but greater than those of Cross-sections #5-#16. Figures 4(b)–4(h) show that the addition of R-SED to the bend in the seven runs increased the uniformity of the flow distribution at the concave and convex banks of Cross-sections #5-#26. The

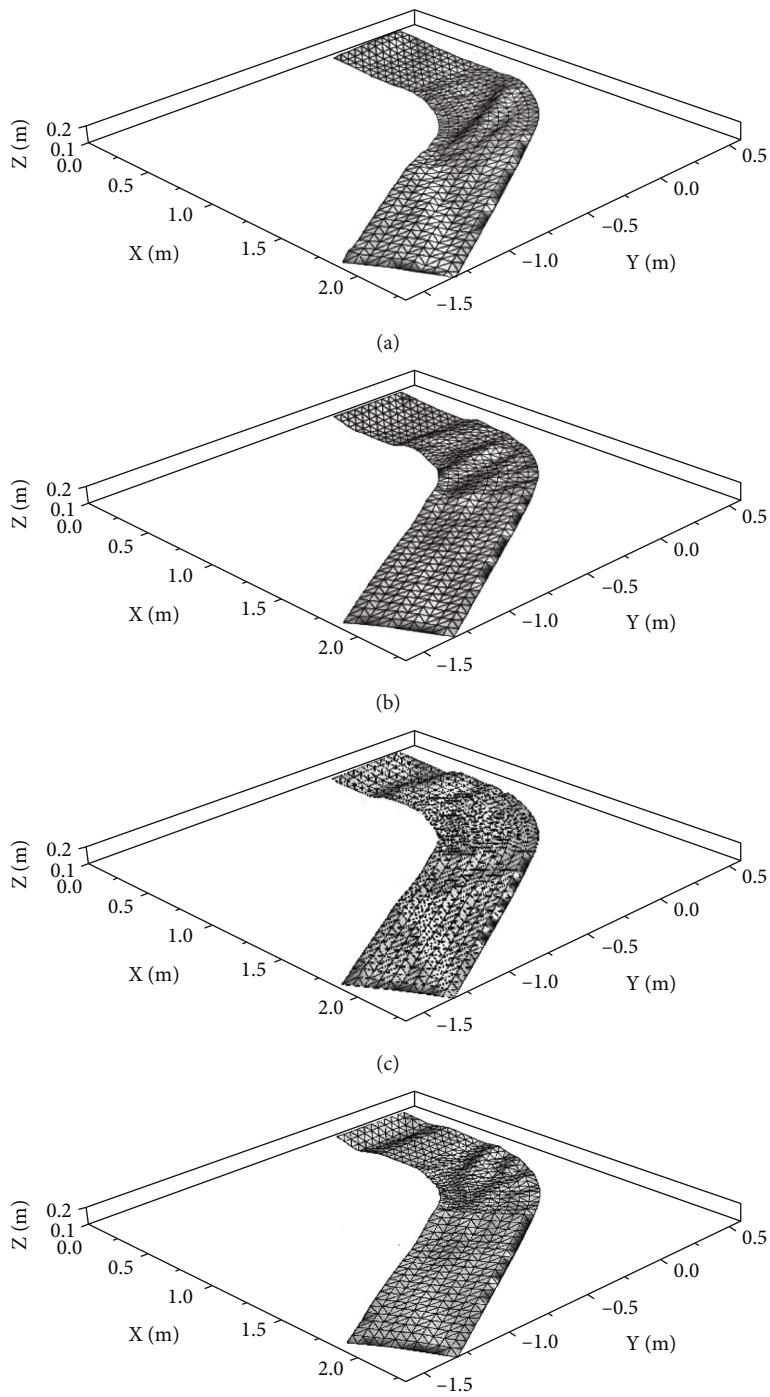

Figure 4: Continued.

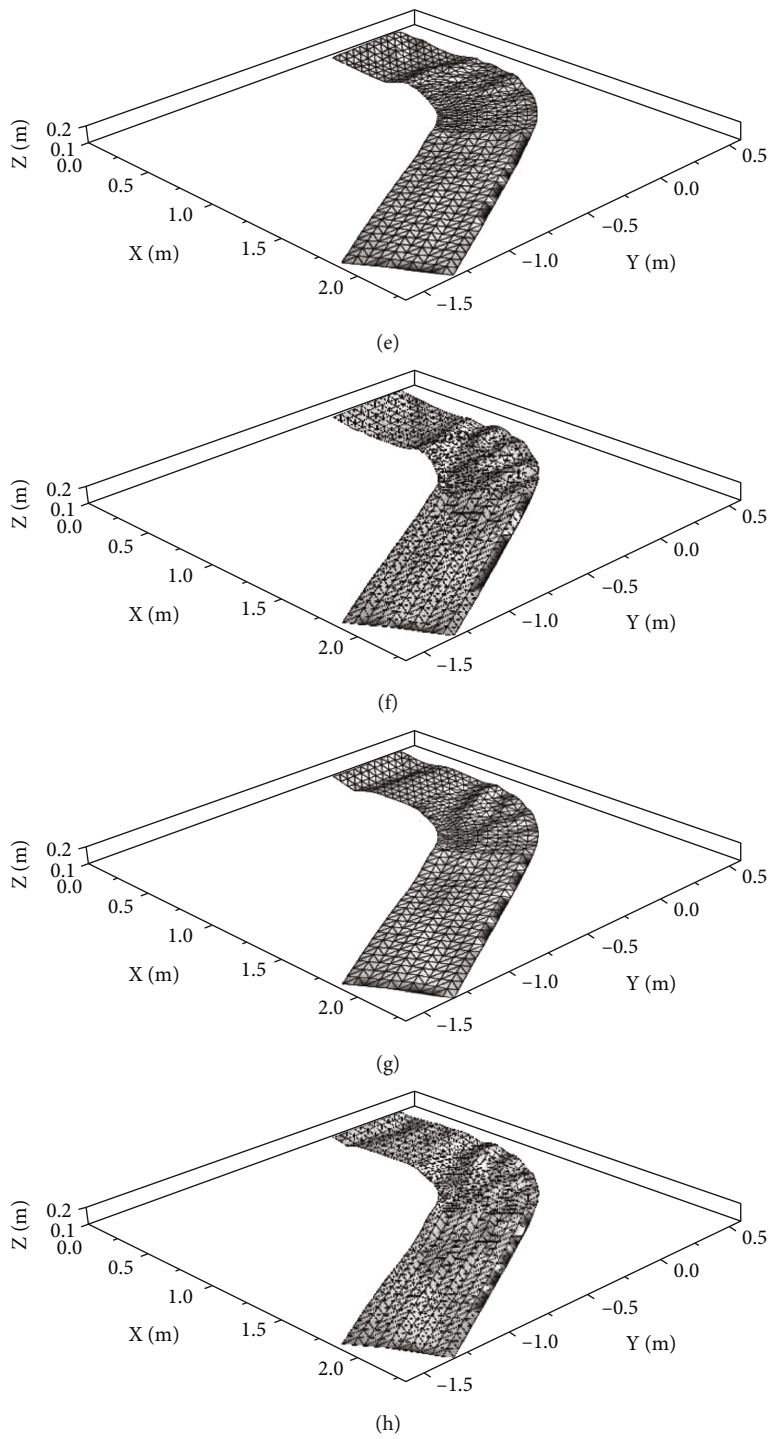

Figure 4: Comparison of the flow patterns in the runs with and without R-SEDs in the spillway. (a) Run 0 (without R-SEDs); (b) Run 1; (c) Run 4; (d) Run 7; (e) Run 10; (f) Run 13; (g) Run 16; (h) Run 19.

comparison with Figure 4(a) shows that the arrangement of R-SEDs significantly reduced the overall water-surface fluctuation (i.e., the water depth at each cross-section varied greatly, with a wavy water surface) of the bend and the water surface difference between the concave and convex banks. The water flow distribution at each cross-section in the straight section of the downstream outlet tended to be uniform, and there was no undesirable flow pattern. This shows that the R-SEDs had excellent flow diversion and stabilization effects. Comparing the flow patterns of the spillway in these eight runs, Figure 4(h) shows that Run 19 showed the most stable water surface structure (with an overall steady water flow pattern, uniform water flow distribution at each cross-section, and a small water surface fluctuation) in the spillway bend section and the straight section of the downstream outlet.

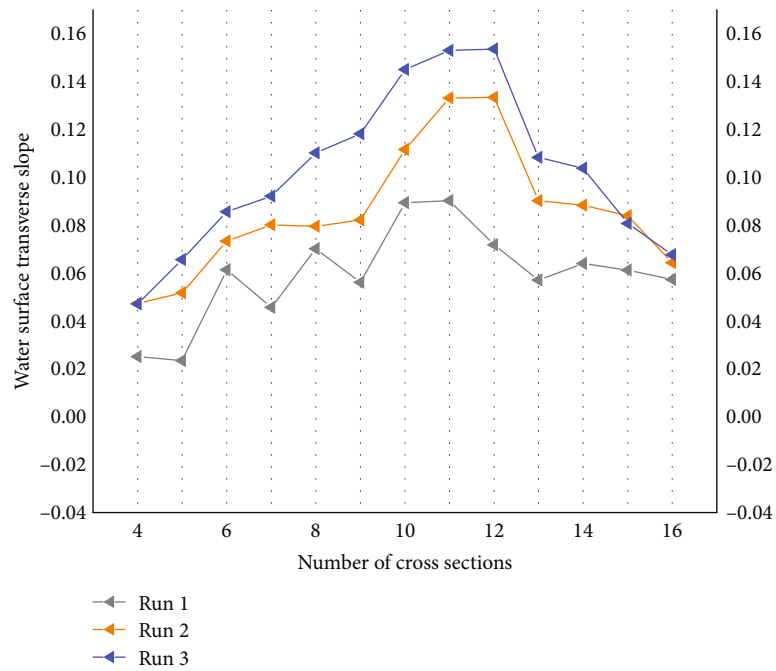

(a)

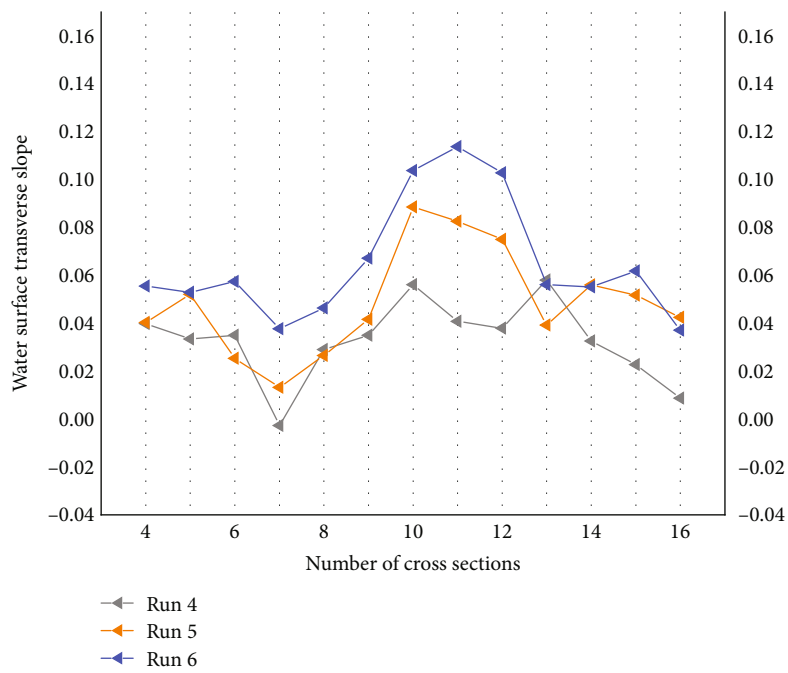

(b)

Figure 5: Continued.

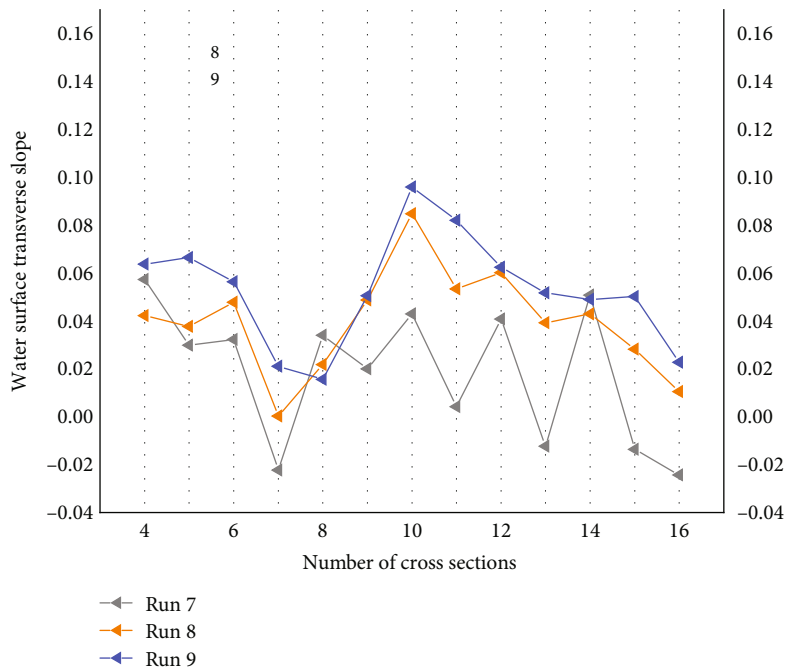

(c)

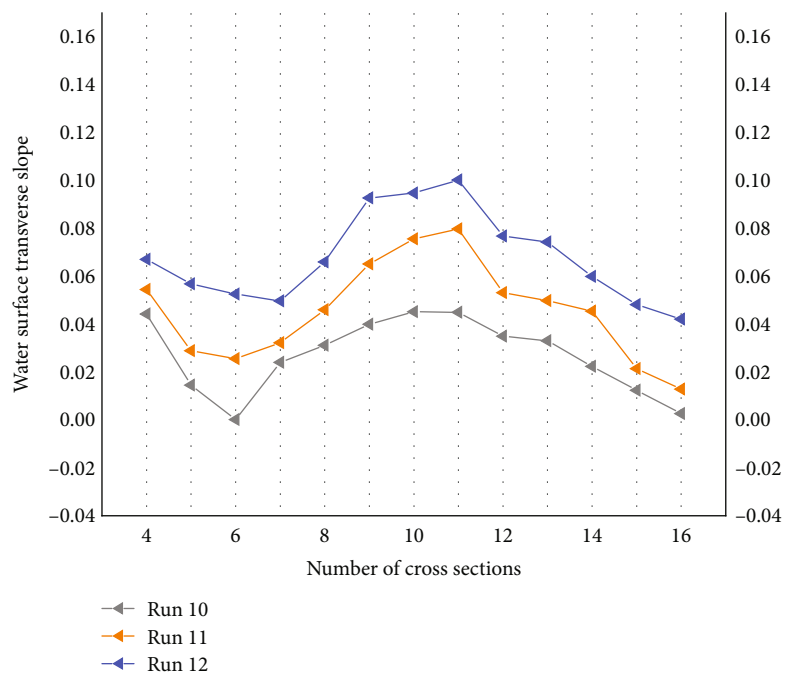

(d)

Figure 5: Continued.

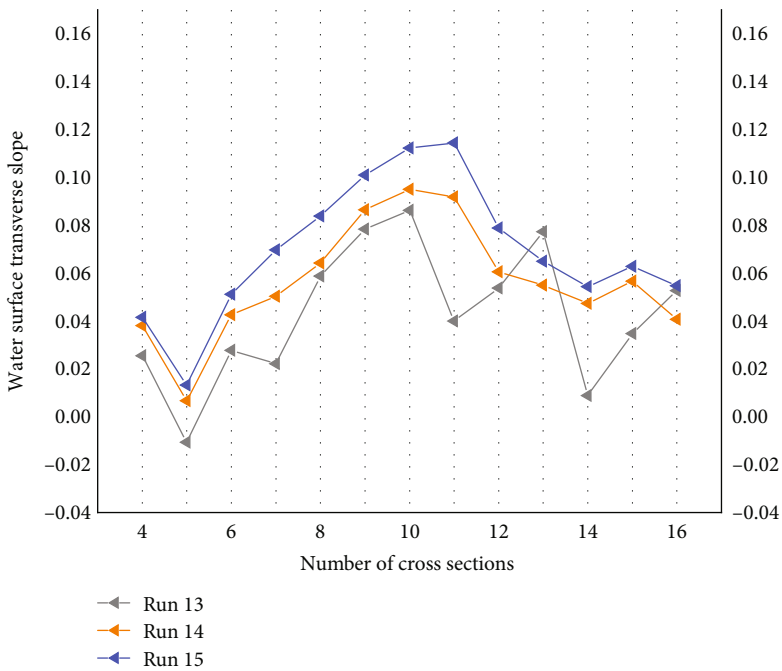

(e)

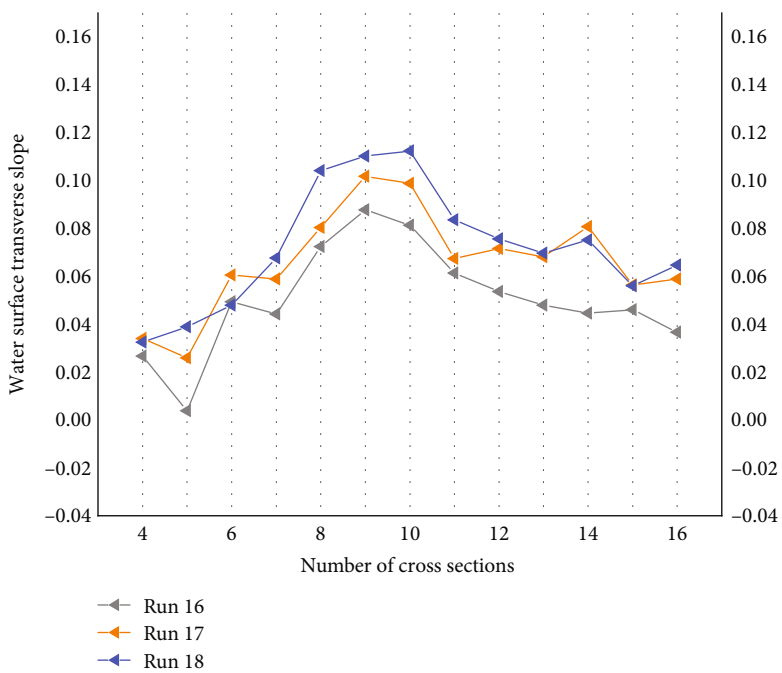

(f)

Figure 5: Continued.

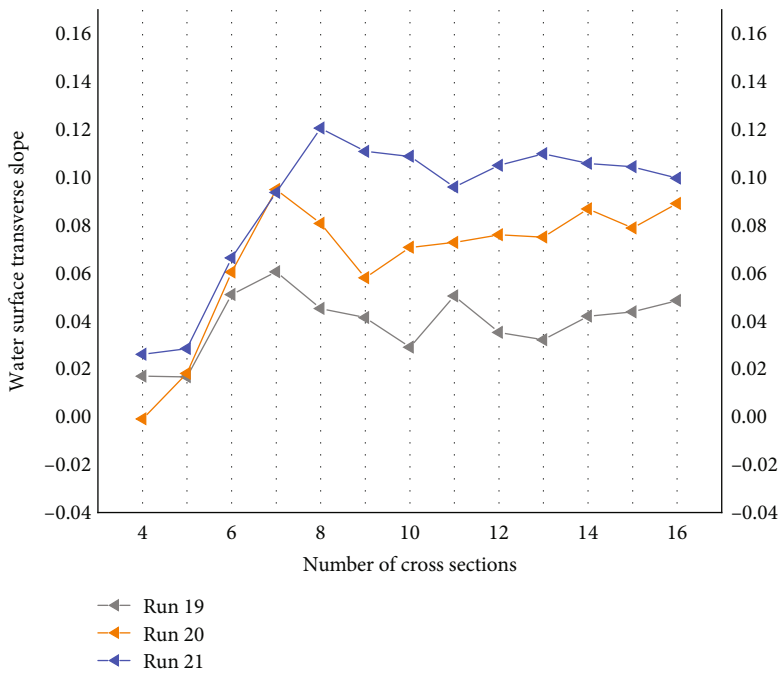

(g)

Figure 5: Distribution of water surface transverse slope in the curved spillway in 21 runs. (a) Runs 1-3; (b) Runs 4-6; (c) Runs 7-9; (d) Runs 10-12; (e) Runs 13-15; (f) Runs 16-18; (g) Runs 19-21.

3.2. Water Surface Transverse Slope. The water surface transverse slope is the gradient of the water surface perpendicular to the mainstream direction, which mainly occurs in the bend due to the centrifugal inertial force of the flow. It can quantify the uniformity of the flow distribution at the concave and convex banks. In different flow runs, with the increase of the discharge flow rate, the water depth in the curved spillway increased, while the average flow velocity and the centrifugal inertial force decreased. Thus, the water surface transverse slope characteristics at the same position were affected. The water surface transverse slope can be calculated using

$$J = \frac{Z_{cc} - Z_{cv}}{B}, \tag{3}$$

where Z_{cc} and Z_{cv} are the water depth at the concave and convex banks (m), respectively, and B is the bend width (taken as 0.5 m in this study) (m).

Equation (3) was applied to calculate the water surface transverse slopes of Cross-sections #4-#16 of the bend. Figure 5 shows the variation of the water surface transverse slope along the bend in the 21 runs. Figures 5(a)–5(g) shows that with the same R-SED arrangement, the water surface transverse slope at the same position was larger at a larger discharge flow rate. In the three runs with different flow rates, when the discharge flow rate was 15 L/s, the overall water surface transverse slope was small and uniformly distributed along the flow path. The water surface transverse slope changed along the longitudinal flow, formed at the entrance to the bend, and reached the maximum near the middle section (Cross-section #10) of the bend. Subsequently, the water surface transverse slope decreased gradually. The water surface transverse slope decreased with the increase of the R-SED height while showing a trend of uniform distribution with the increase of the R-SED angle. In addition, when $\Delta L = 17$ cm, the water surface transverse slope distribution along the bend was relatively uniform. Figure 5(g) shows that the maximum water surface transverse slope (i.e., 0.1206) occurred in Cross-section #8 in Run 21.

3.3. Free-Surface Longitudinal Profile. The free-surface longitudinal profile can effectively describe the degree of water surface changes along the spillway. The free-surface longitudinal profiles of the spillway in the 21 runs are shown in Figure 6. In this study, the dimensionless water depth was used to analyze the free-surface longitudinal profile, which was expressed as the ratio of actual water depth (H) to critical water depth (H_c), i.e., H/H_c.

Runs 1, 2, and 3 were selected as examples to demonstrate the test results. Figure 6(a) indicates that with the same R-SED arrangement ($h_1/h_2 = 1.0$ cm/1.5 cm, $\theta = 20\circ$, and $\Delta L = 17$ cm), the variation of the water depth along the spillway in Run 1 ($Q = 15$ L/s) was relatively small. Similarly, in other runs with the same R-SED arrangement, the fluctuation of the free-surface longitudinal profile in the bend section increased with the increase of the discharge flow rate. Runs 1, 4, and 7 were compared in Figures 6(a)–6(c). In Run 4 ($h_1/h_2 = 1.5$ cm/0.75 cm), the variation of the water depth along the bend section was the smallest, and 1.5 cm/0.75 cm was the optimal height of the R-SED. Runs 4, 10, and 13 with different spacing of R-SEDs were compared in Figures 6(b), 6(d), and 6(e). The variation of the water depth along the bend

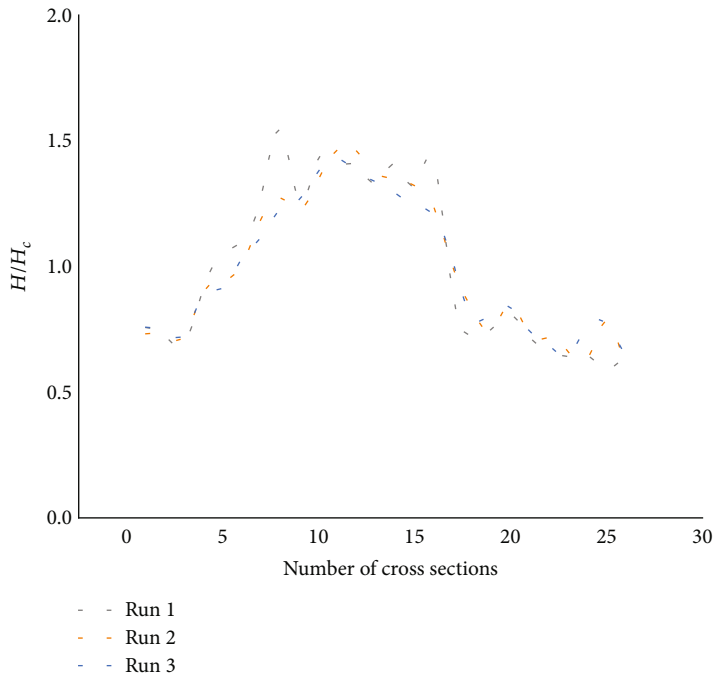

(a)

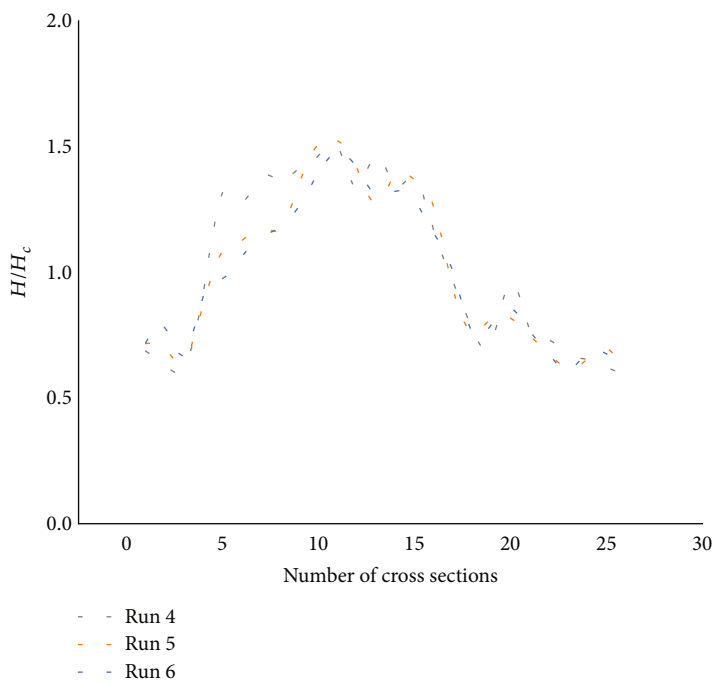

(b)

Figure 6: Continued.

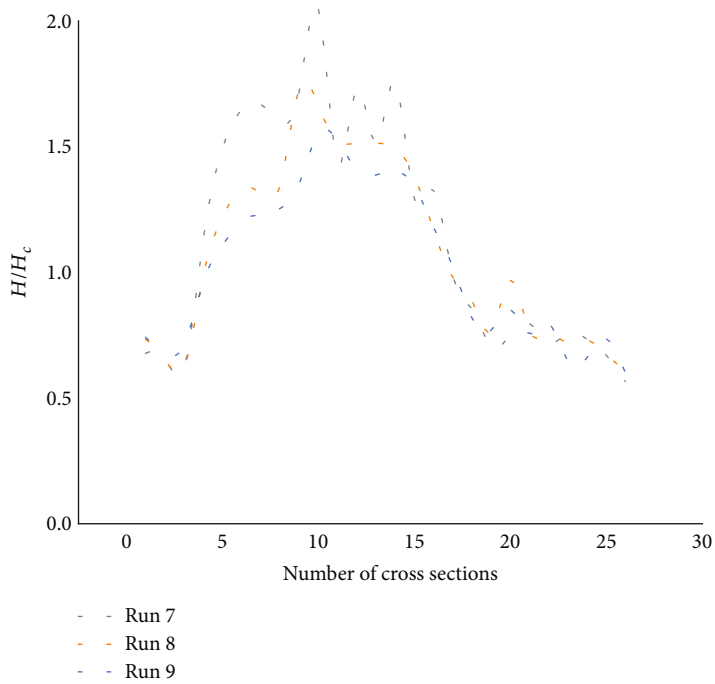

(c)

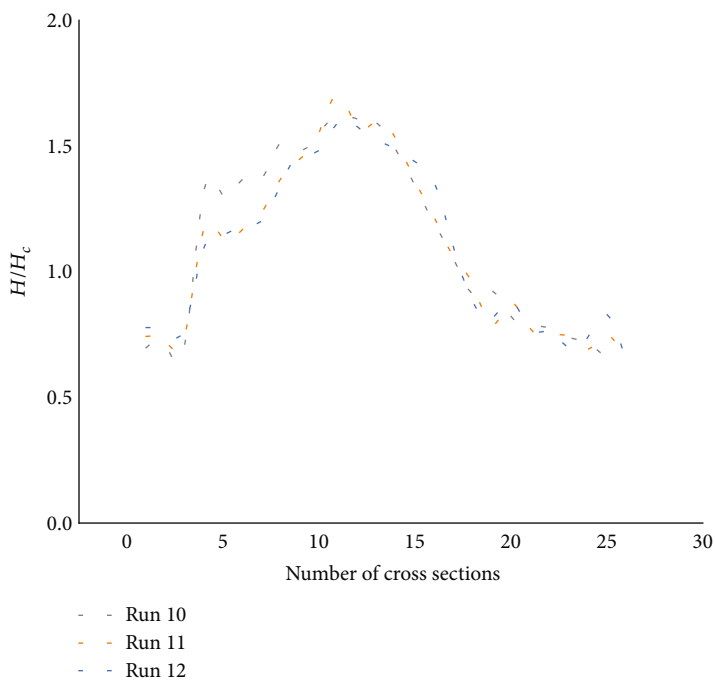

(d)

Figure 6: Continued.

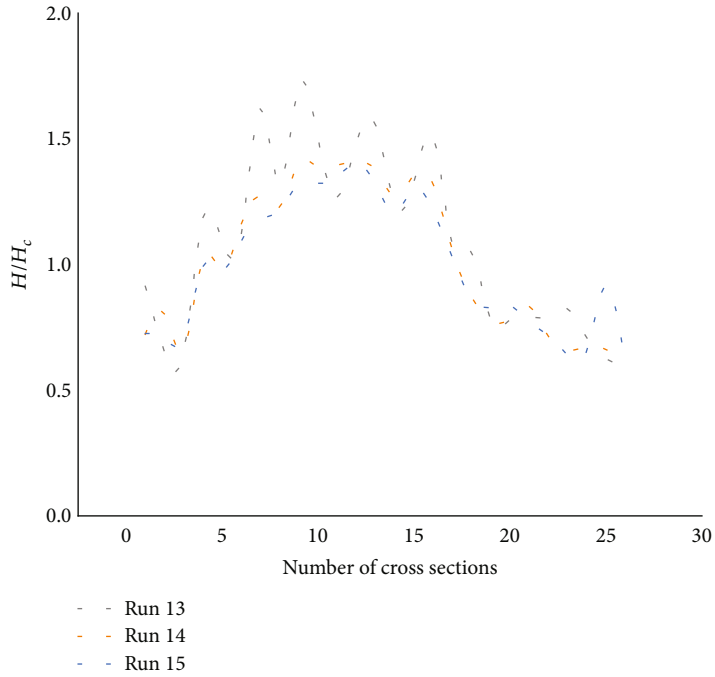

(e)

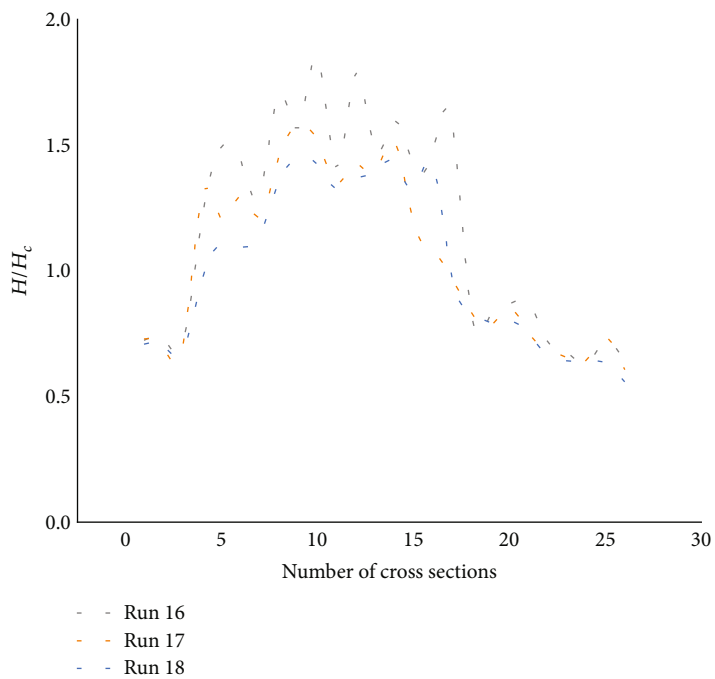

(f)

Figure 6: Continued.

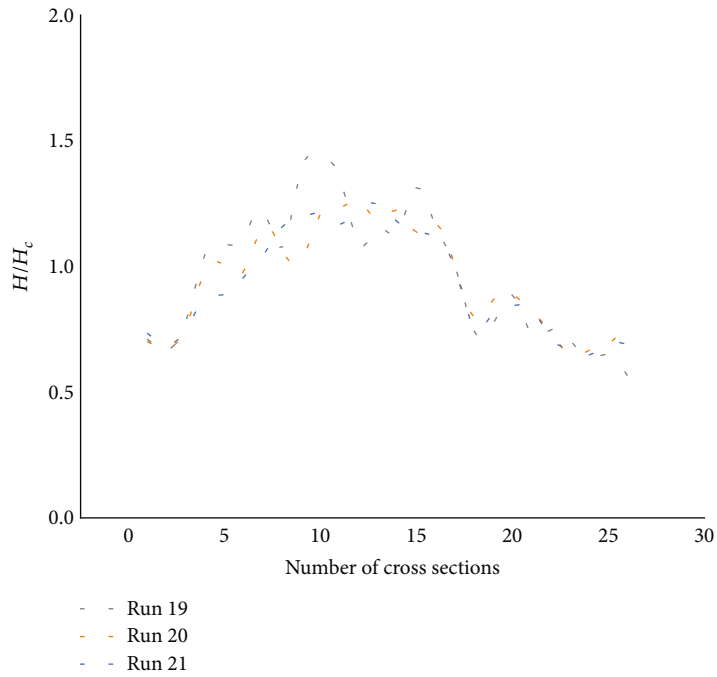

(g)

Figure 6: Free-surface longitudinal profiles of the curved spillway in the 21 runs. (a) Runs 1-3; (b) Runs 4-6; (c) Runs 7-9; (d) Runs 10-12; (e) Runs 13-15; (f) Runs 16-18; (g) Runs 19-21.

section in Run 4 ($\Delta L = 17$ cm) was the smallest. This indicates that 17 cm was the optimal spacing of the R-SEDs. Runs 4, 16, and 19 with different angles of R-SEDs were compared in Figures 6(b), 6(f), and 6(g). Run 19 ($\theta = 40°$) showed the smallest water depth variation along the bend section, indicating that 40° was the optimal angle of the R-SEDs.

3.4. Cross-Sectional Velocity Distribution. The cross-sectional velocity distribution patterns of the bend flow are the basis for studying the bend flow movement. Typical Runs 1, 4, 7, 10, 13, 16 and 19, with better water surface structure improvement effects in the curved spillway, were selected. Typical Cross-sections #4, #7, #10 (the middle cross-section of the bend), #13, #16, #19, #22, and #25 were selected for comparative analysis. Figure 7 presents the cross-sectional velocity distributions. In this study, the dimensionless flow velocity was used to analyze the cross-sectional velocity distribution, which was expressed as the ratio of actual flow velocity (v) to critical flow velocity (v_c), i.e., v/v_c.

Figure 7(a) shows that in the seven typical runs, the dimensionless flow velocity at Cross-section #4 (at the bend inlet) ranged between 50 and 100. Compared with other sections, Cross-section #4 had the smallest difference between the dimensionless flow velocity at the convex and concave banks, with relative uniform velocity distribution. Figures 7(b)–7(e) show that compared with the velocity at Cross-section #4, the dimensionless flow velocity at Cross-sections #7, #10, #13, and #16 in the bend section showed an overall decreasing trend and generally ranged between 20 and 80. The average dimensionless flow velocity was reduced by 37.9%, while the velocity showed an increased fluctuation degree and overall wavy distribution. Particularly, the dimensionless flow velocity at Cross-section #10 (the middle cross-section of the bend) had the largest decrease by 51.9%. This was because the arrangement of R-SEDs at the bottom of the bend increased its roughness. The original continuous and straight water flow was disrupted, thus increasing the number of collisions between water flows and causing energy dissipation. Thus, the flow velocity was reduced. By comparing Runs 1, 4, and 7, increasing the height of the R-SEDs can effectively reduce the flow velocity. However, excessive or too small height of the R-SED did not show clear reduction effects on the flow velocity. Based on the comparison of Runs 4, 10, and 13, increasing the spacing between adjacent R-SEDs can promote water turbulence and reduce the flow velocity. However, excessive or too small spacing is not conducive to water turbulence and swirling. Runs 4, 16, and 19 were compared using the same arrangement of the R-SED, such as the optimal height (1.5 cm/0.75 cm), spacing (17 cm), and discharge flow rate (15 L/s). When the angle of the R-SED was 40° (Run 19), the flow velocity at each measurement cross-section decreased significantly, with high distribution uniformity. Figures 7(f)–7(h) shows that compared with the cross-sections (i.e., #7, #10, #13, and #16) at the bend section, the cross-sections (i.e., #19, #22, and #25) at the straight outlet section showed an increasing trend in the dimensionless flow velocity. The dimensionless flow velocity ranged between 40 and 120, with an increase in the average value by 37.5%. The fluctuation degree of the cross-sectional flow velocity gradually decreased. The cross-sectional velocity distribution was more uniform when the water flow was closer to the outlet. This indicates that the installation of R-

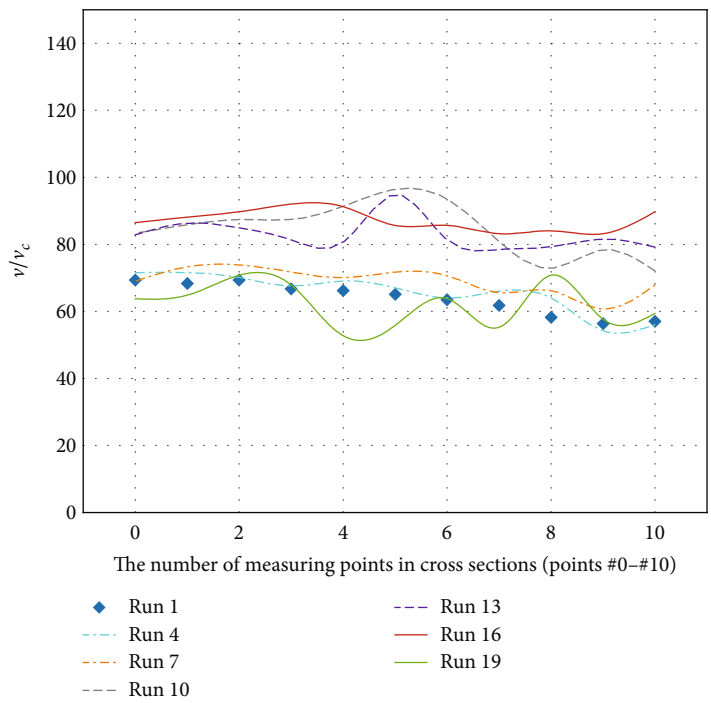

(a)

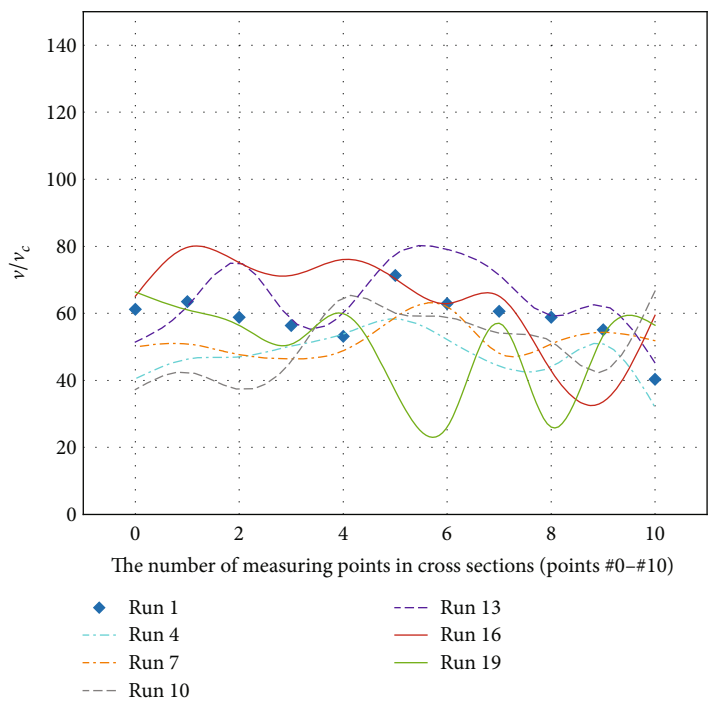

(b)

Figure 7: Continued.

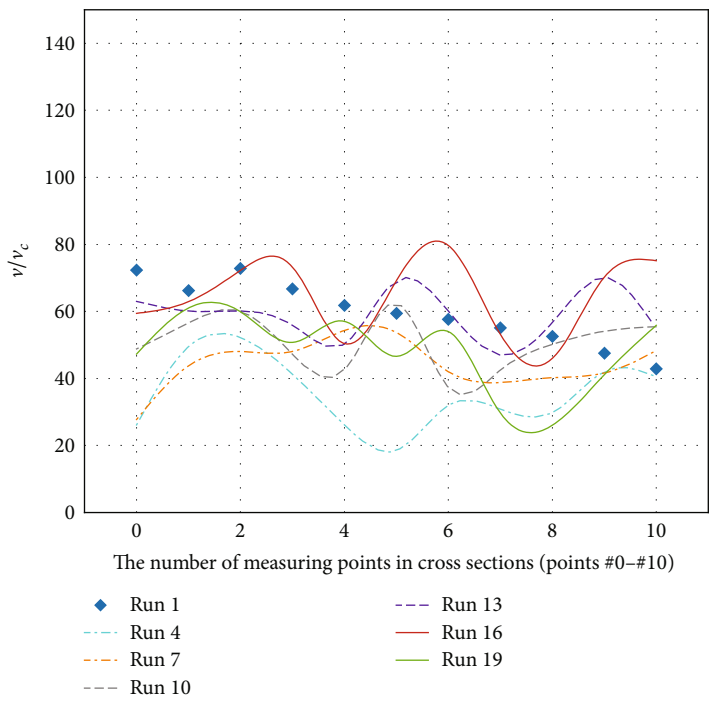

(c)

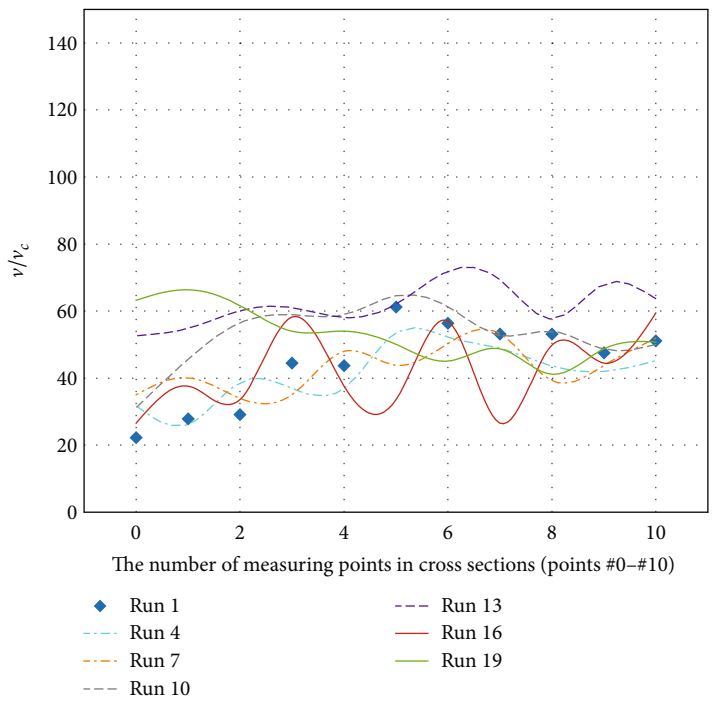

(d)

Figure 7: Continued.

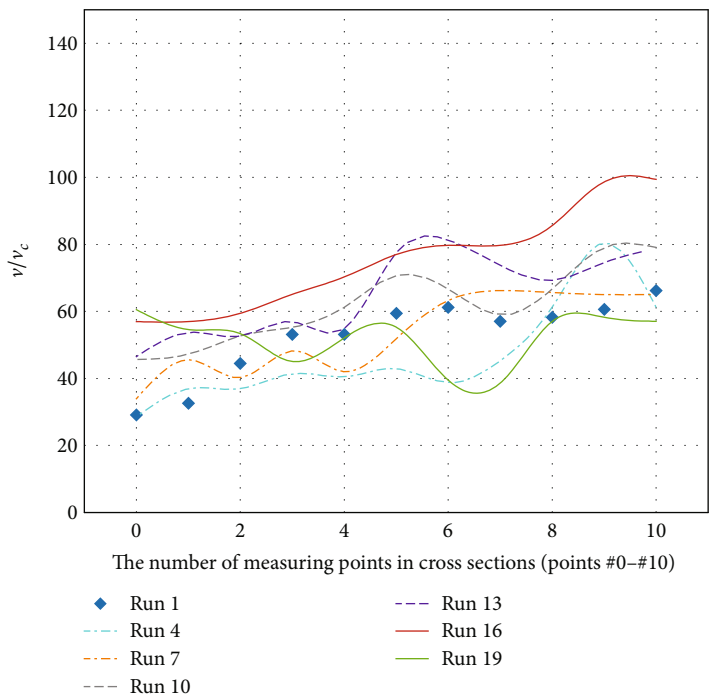

(e)

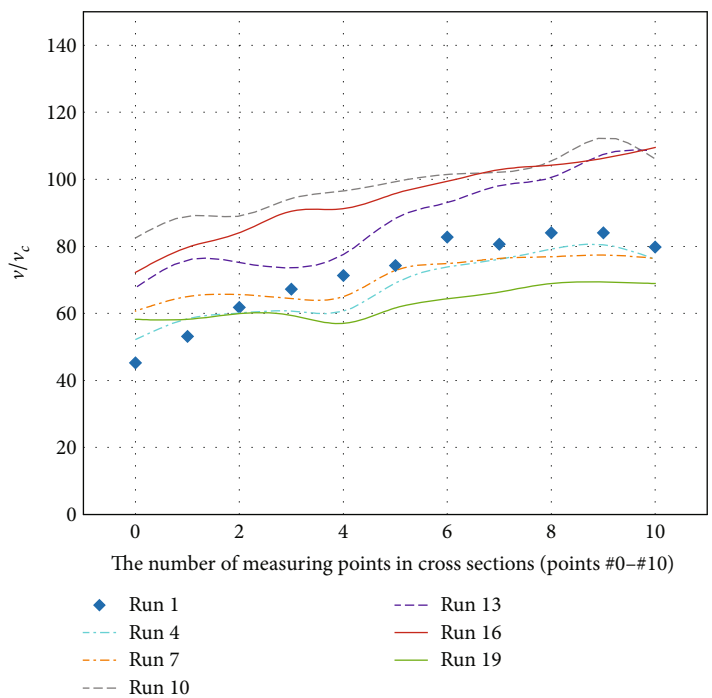

(f)

Figure 7: Continued.

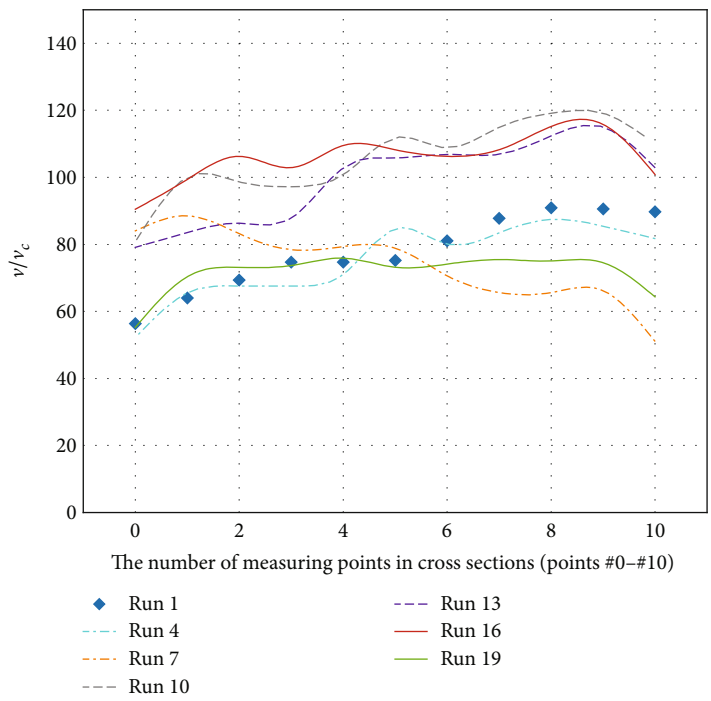

(g)

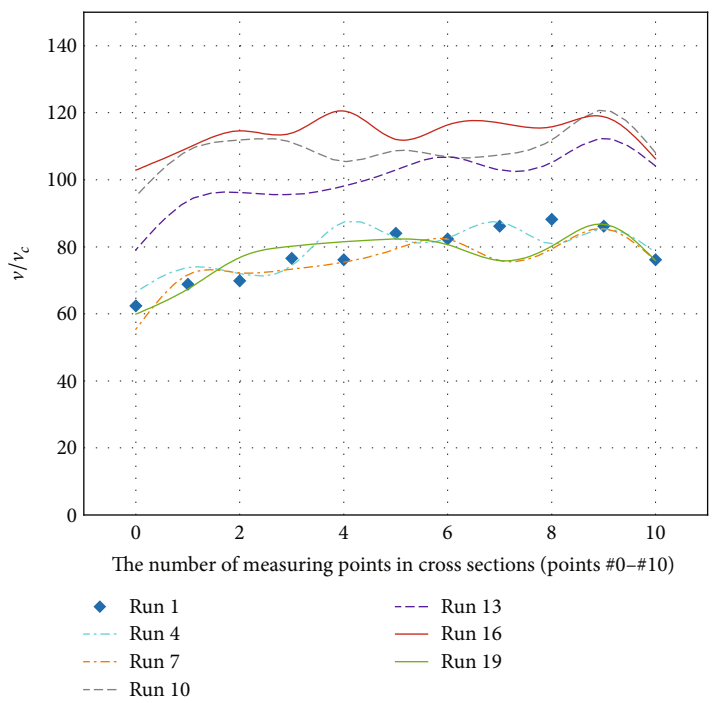

(h)

Figure 7: Typical cross-sectional velocity distribution of the spillway in the typical runs: Cross-sections (a) #4, (b) #7, (c) #10, (d) #13, (e) #16, (f) #19, (g) #22, and (h) #25.

SEDs in the bend section can properly regulate the flow in the straight section of the downstream outlet.

3.5. Analysis of Energy Dissipation Rate. After the R-SEDs were installed, the water flow between adjacent R-SEDs in the bend was disrupted, causing flow mixing and collision. The shear force was generated. Then, different-scale vortex flows occurred, thus resulting in energy dissipation. A schematic diagram of the R-SED energy dissipation process is shown in Figure 8. With the installation of the R-SED at the bottom of the bend with a certain slope i, most of the energy of the discharge flow was dissipated in the form of

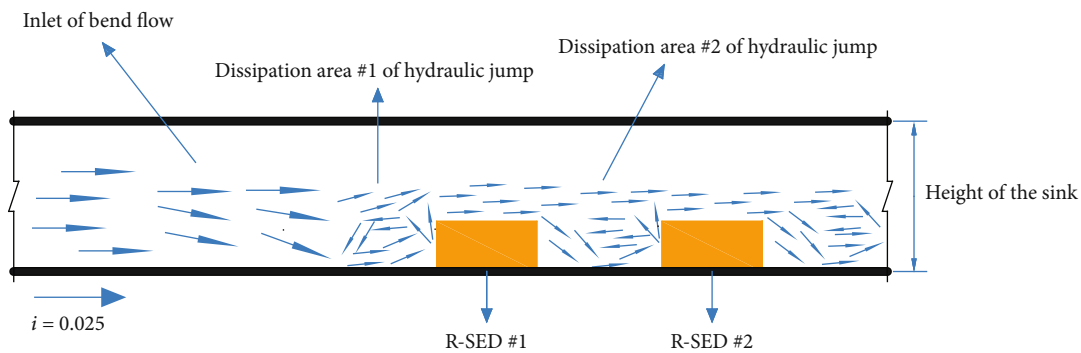

Figure 8: Schematic diagram of the energy dissipation process of the R-SEDs.

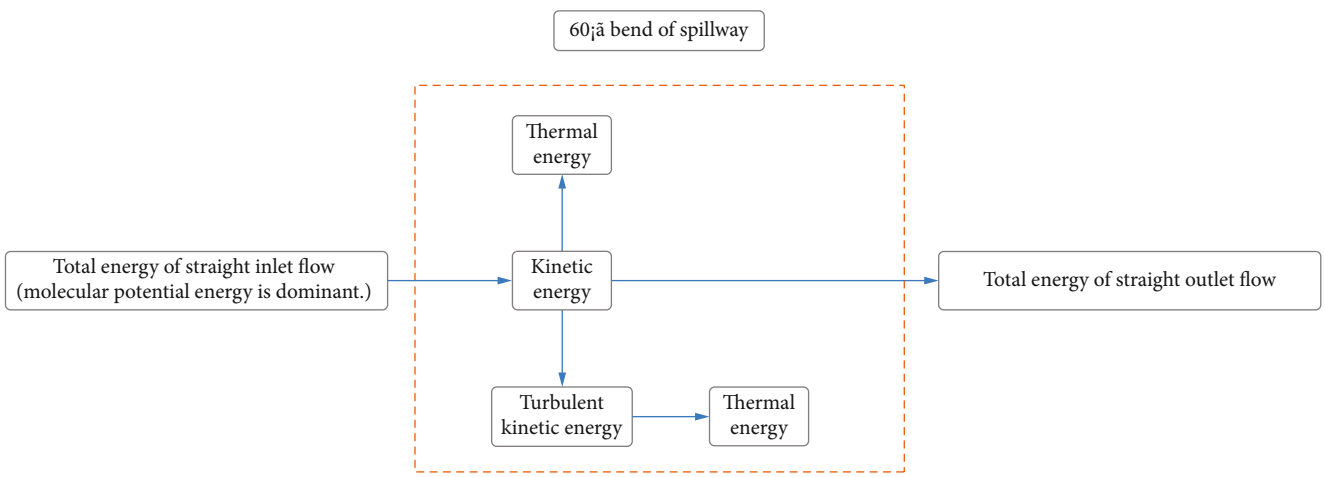

Figure 9: Schematic diagram of the energy dissipation process of the R-SEDs.

turbulence, and kinetic energy was the main source of turbulent kinetic energy. The release of potential energy could continuously replenish the flow and provide kinetic energy. After entering the bend, the flow hit the water surface of R-SED #1, forming dissipation area #1 of the hydraulic jump in this section. Then, the top water flow climbed over the top of R-SED #1 and entered dissipation area #2 of the hydraulic jump. The water flow continued to roll and jump again to form large and small whirlpools. Thus, the top water continuously flowed over the top of R-SED #2. Then, a continuous energy dissipation process was formed at the 60° bend, with a better energy dissipation effect.

When the flow entered the bend for energy dissipation, a multistage energy conversion process occurred, mainly including step-by-step conversion of kinetic energy, potential energy, turbulent kinetic energy, and thermal energy (Figure 9). Figures 8 and 9 show that the inlet water flowed down the straight inlet section of the spillway and then the potential energy of the flow was converted into kinetic energy. Subsequently, the flow entered the bend and hit the water surface of the R-SEDs, resulting in energy dissipation of the hydraulic jump. There was a flow velocity gradient between the dissipation area of the hydraulic jump, the main flow area, and the boundary area of the surrounding water body. Thus, a large amount of kinetic energy was converted into turbulent kinetic energy. In addition, some air was mixed into the water tongue between adjacent R-SEDs during disruption, resulting in enhanced water turbulence and intense energy dissipation. When the water flowed out of the bend, turbulent kinetic energy was gradually dissipated into heat energy, and kinetic energy was gradually recovered. Then, the energy conversion in the energy dissipation process of the R-SEDs was completed.

The energy dissipation rate was used to quantify the energy dissipation effect of R-SEDs in the continuous energy dissipation process. The energy dissipation rates of the 21 runs were calculated using

$$\eta = \frac{E_i - E_j}{E_i} \times 100\%,$$
$$E_i = Z_i + H_i + \frac{\alpha_i v_i^2}{2g}, \tag{4}$$
$$E_j = Z_j + H_j + \frac{\alpha_j v_j^2}{2g},$$

where η is the energy dissipation rate (%), E_i is the total energy in the inlet section of the bend (m), Z_i is the lowest elevation in the inlet section (m), H_i is the average water depth in the inlet section (m), v_i is the average flow velocity in the inlet section (m/s), and α_i and α_j are the kinetic energy

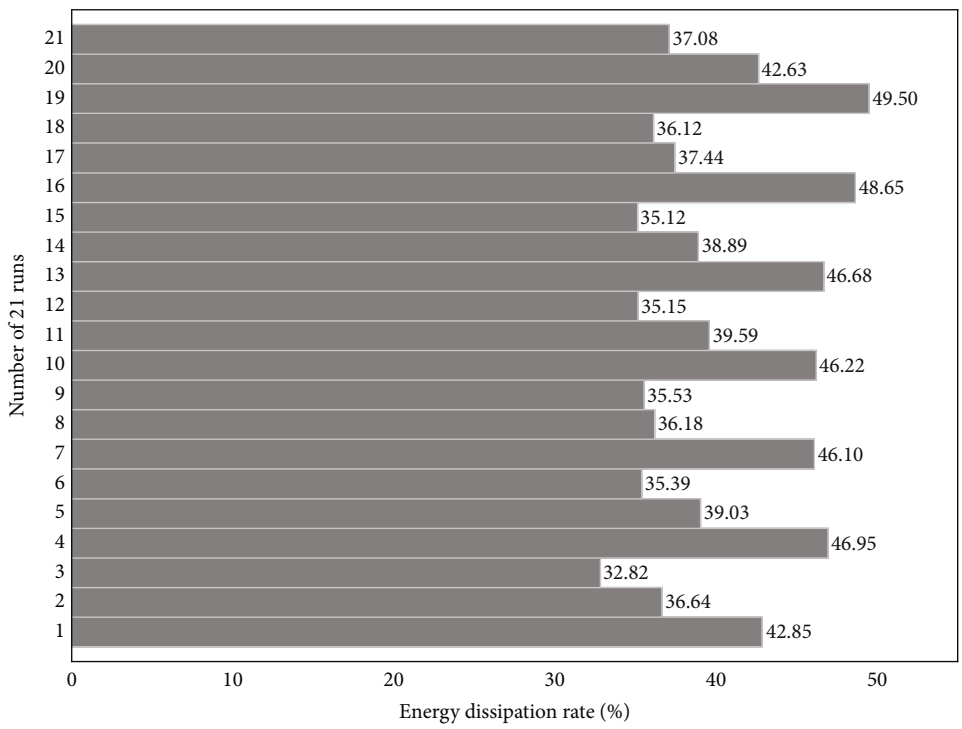

Figure 10: Calculated energy dissipation rates of the R-SEDs in the 21 runs.

correction coefficients ($\alpha_i, \alpha_j = \int_A u^3 dA/v^3 A$. α_i and α_j depend on the flow velocity distribution at the flow cross-section; for the gradually varied flow, $\alpha_i, \alpha_j = 1.0{\sim}1.05$ and are commonly taken as 1.0 in engineering practice; in this paper, the bend flow in the spillway belonged to a nonuniform gradually-varied flow; Thus, α_i and α_j were taken as 1.0.), E_j is the total energy in the outlet section of the bend (m), Z_j is the lowest elevation in the outlet section (m), H_j is the average water depth in the outlet section (m), and v_j is the average flow velocity in the outlet section (m/s).

The energy dissipation rates of the R-SED in the 21 runs were calculated, and the results are shown in Figure 10. The energy dissipation rates ranged between 30% and 50%. With the same arrangement of R-SEDs, the energy dissipation rate was generally the highest (above 45%) at $Q = 15$ L/s, with a maximum of 49.5% (Run 19). When Q increased to 25 and 35 L/s, the energy dissipation rate decreased by about 15%-30% and 30%-35%, respectively. With the increase in the discharge flow rate, the energy dissipation rate tended to decrease.

According to the above results, Run 19 showed the largest improvement in the bend flow ($Q = 15$ L/s, arrangement of the R-SEDs: $h_1/h_2 = 1.5$ cm/0.75 cm, $\Delta L = 17$ cm, and $\theta = 40^\circ$), and the energy dissipation rate was the highest (49.5%).

4. Conclusions

This study is aimed at investigating the effects of the R-SEDs at the bottom of the 60° bend of a curved spillway (with a large width-to-depth ratio) on the bend flow. Based on the hydrodynamic theory and physical model tests, the hydraulic properties of the curved spillway with R-SEDs were studied. The key findings are as follows:

The results of 21 sets of tests reveal that the addition of the R-SED can effectively improve the water surface structure of the spillway and reduce the water depth difference between the two banks of the bend section. The folded water flow disappeared in the downstream straight section. The water surface transverse slope formed at the entrance of the bend and reached the maximum near the middle section of the bend and then gradually decreased. The fluctuations of the free-surface longitudinal profile (i.e., the water depth at each free-surface longitudinal profile varied greatly, with overall wavy distribution) in the bend section increased with the increase in the discharge flow rate.

With the installation of the R-SED to the bend, the bottom roughness of the bend increased. Different water flow layers between adjacent R-SEDs continued to collide and mix, resulting in vortices of different sizes and effective energy dissipation. This resulted in a continuous energy dissipation process, thus reducing the average dimensionless flow velocity in the bend by about 37.9%.

The R-SEDs were simple in shape and easy to construct. The energy dissipation rate of the R-SEDs ranged from 30% to 50%. With the increase in the discharge flow rate, the energy dissipation rate decreased. This will provide a theoretical reference for similar engineering designs.

In the 60° bend of a spillway with a large width-to-depth ratio ($B/H > 5$), the R-SEDs were the most suitable for curved spillways in low-flow runs (15 L/s), compared to those in the runs with high flow rates of 25 and 35 L/s. Among the 21 runs, Run 19 had the largest improvement of the bend flow ($Q = 15$ L/s) and the highest energy dissipation rate (49.5%),

with the following optimal R-SED arrangement: $h_1/h_2 = 1.5$ cm/0.75 cm, $\Delta L = 17$ cm, and $\theta = 40\circ$.

Symbols

i: Slope of spillway
B: Width of bend
H: Water depth
L_1: Length of straight inlet section
S: Total arc length along the center of the bend
R_0: Centerline radius of bend
R_1: Inner diameter of bend
R_2: Outer diameter of bend
s: Transverse flow direction
n: Longitudinal flow direction
h_1: Concave bank height of R-SED
h_2: Convex bank height of R-SED
θ: Angle between the R-SED and the direction of the longitudinal axis of the flow channel
ΔL: Arc distance between the centerlines of adjacent R-SEDs
b: Thickness of an R-SED
l: Longitudinal length of an R-SED
Q: Discharge flow rate of spillway
C_0: Flow coefficient of thin-walled right triangular weir
H_1: Water depth above thin-walled right triangular weir
P_1: Height of thin-walled right triangular weir
B_1: Width of diversion channel upstream of thin-walled right triangular weir
J: Water surface transverse slope
Z_{cc}: Water depth at the concave bank of bend
Z_{cv}: Water depth at the convex bank of bend
H_c: Critical water depth
v: Flow velocity
v_c: Critical flow velocity
η: Energy dissipation rate of R-SED
E_i: Total energy in the inlet section of bend
Z_i: Lowest elevation in the inlet section of bend
H_i: Average water depth in the inlet section of bend
v_i: Average flow velocity in the inlet section of bend
α_i, α_j: Kinetic energy correction coefficient
E_j: Total energy in the outlet section of bend
Z_j: Lowest elevation in the outlet section of bend
H_j: Average water depth in the outlet section of bend
v_j: Average flow velocity in the outlet section of bend.

Data Availability

The data used to support the findings of this study are included within the article.

Conflicts of Interest

The authors declare that there is no conflict of interest regarding the publication of this paper.

Acknowledgments

The writers gratefully acknowledge the financial support from the National Natural Science Foundation of China (Grant No. 51769037) and the Xinjiang Uygur Autonomous Region University Research Program Innovation Team Project (Grant No. XJEDU2017T004).

References

[1] S. Damarnegara, W. Wardoyo, R. Perkins, and E. Vincens, "Computational fluid dynamics (cfd) simulation on the hydraulics of a spillway," *IOP Conference Series: Earth and Environmental Science.*, vol. 437, no. 1, article 012007, 2020(6pp).

[2] C. S. James, *Hydraulic Structures*, Springer, 2020.

[3] J. A. Kells and C. D. Smith, "Reduction of cavitation on spillways by induced air entrainment," *Canadian Journal of Civil Engineering*, vol. 18, no. 3, pp. 358–377, 1991.

[4] Q. Zhang, Y. Diao, X. Zhai, and S. Li, "Experimental study on improvement effect of guide wall to water flow in bend of spillway chute," *Water Science and Technology*, vol. 73, no. 3, pp. 669–678, 2016.

[5] H. Chanson, *Energy Dissipation in Hydraulic Structures*, CRC Press, Taylor and Francis Group, Leiden. The Netherlands, IAHR Monograph, 2015.

[6] I. W. Seo and J. Shin, "Two-dimensional modeling of flow and contaminant transport in meandering channels," *EPiC Series in Engineering*, vol. 3, pp. 1911–1918, 2009.

[7] J. Yang, J. Zhang, Q. Zhang, X. Teng, W. Chen, and X. Li, "Experimental research on the maximum backwater height in front of a permeable spur dike in the bend of a spillway chute," *Water Supply*, vol. 19, no. 6, pp. 1841–1850, 2019.

[8] P. Parsapour-moghaddam and C. Rennie, "Influence of meander confinement on hydro-morphodynamics of a cohesive meandering channel," *Water*, vol. 10, no. 4, p. 354, 2018.

[9] N. R. B. Olsen, "Three-dimensional CFD modeling of self-forming meandering channel," *Journal of Hydraulic Engineering*, vol. 129, no. 5, pp. 366–372, 2003.

[10] J. Thomson, "On the origin of windings of rivers in alluvial plains, with remarks on the flow of water round bends in pipes," *Proceedings of the Royal Society of London*, vol. 25, no. 171-178, pp. 5–8, 1877.

[11] J. S. Maatooq and L. K. Hameed, "2D model to investigate the morphological and hydraulic changes of meanders," *Engineering and Technology Journal*, vol. 38, pp. 9–19, 2020.

[12] C. Qin, X. Shao, and G. Zhou, "Comparison of two different secondary flow correction models for depth-averaged flow simulation of meandering channels," *Procedia Engineering*, vol. 154, pp. 412–419, 2016.

[13] O. Seyedashraf and A. A. Akhtari, "Flow separation control in open-channel bends," *Journal of the Chinese Institute of Engineers*, vol. 39, no. 1, pp. 40–48, 2016.

[14] J. Zhou, X. Shao, H. Wang, and D. Jia, "Assessment of the predictive capability of RANS models in simulating meandering open channel flows," *Journal of Hydrodynamics, Ser. B*, vol. 29, no. 1, pp. 40–51, 2017.

[15] S. S. Han, A. S. Ramamurthy, and P. M. Biron, "Characteristics of flow around open channel 90° bends with vanes," *Journal of Irrigation and Drainage Engineering*, vol. 137, no. 10, pp. 668–676, 2011.

[16] C. Hu, M. Yu, H. Wei, and C. Liu, "The mechanisms of energy transformation in sharp open-channel bends: analysis based on experiments in a laboratory flume," *Journal of Hydrology*, vol. 571, pp. 723–739, 2019.

[17] J. S. Kim, D. Baek, and I. Park, "Evaluating the impact of turbulence closure models on solute transport simulations in meandering open channels," *Applied Sciences*, vol. 10, no. 8, p. 2769, 2020.

[18] I. J. Moncho-Esteve, M. García-Villalba, Y. Muto, K. Shiono, and G. Palau-Salvador, "A numerical study of the complex flow structure in a compound meandering channel," *Advances in Water Resources*, vol. 116, pp. 95–116, 2018.

[19] A. Pradhan, K. Kumar Khatua, and S. Sankalp, "Variation of velocity distribution in rough meandering channels," *Advances in Civil Engineering*, vol. 2018, Article ID 1569271, 12 pages, 2018.

[20] H. K. Schreiner, C. D. Rennie, and A. Mohammadian, "Trajectory of a jet in crossflow in a channel bend," *Environmental Fluid Mechanics*, vol. 18, no. 6, pp. 1301–1319, 2018.

[21] M. Vaghefi, M. Akbari, and A. R. Fiouz, "An experimental study of mean and turbulent flow in a 180 degree sharp open channel bend: secondary flow and bed shear stress," *KSCE Journal of Civil Engineering*, vol. 20, no. 4, pp. 1582–1593, 2016.

[22] X. Yan, C. D. Rennie, and A. Mohammadian, "A three-dimensional numerical study of flow characteristics in strongly curved channel bends with different side slopes," *Environmental Fluid Mechanics*, vol. 20, no. 6, pp. 1491–1510, 2020.

[23] R. Booij, "Measurements and large eddy simulations of the flows in some curved flumes," *Journal of Turbulence*, vol. 4, no. 1, 2003.

[24] F. L. Engel and B. L. Rhoads, "Three-dimensional flow structure and patterns of bed shear stress in an evolving compound meander bend," *Earth Surface Processes and Landforms*, vol. 41, no. 9, pp. 1211–1226, 2016.

[25] L. Gu, S. Zhang, L. He et al., "Modeling flow pattern and evolution of meandering channels with a nonlinear model," *Water*, vol. 8, no. 10, p. 418, 2016.

[26] W. Huai, C. Li, Y. Zeng, Z. Qian, and Z. Yang, "Curved open channel flow on vegetation roughened inner bank," *Journal of Hydrodynamics*, vol. 24, no. 1, pp. 124–129, 2012.

[27] A. S. Ramamurthy, S. S. Han, and P. M. Biron, "Three-dimensional simulation parameters for 90° open channel bend flows," *Journal of Computing in Civil Engineering*, vol. 27, no. 3, pp. 282–291, 2013.

[28] R. Shaheed, A. Mohammadian, and X. Yan, "A review of numerical simulations of secondary flows in river bends," *Water*, vol. 13, no. 7, p. 884, 2021.

[29] R. Ranjan, Z. Ahmad, and G. L. Asawa, "Effect of spacing of submerged vanes on bed scour around river bends," *ISH Journal of Hydraulic Engineering*, vol. 12, no. 2, pp. 49–65, 2006.

[30] J. P. Martín-Vide, M. Roca, and C. A. Alvarado-Ancieta, "Bend scour protection using riprap," *Proceedings of the Institution of Civil Engineers-Water Management*, vol. 163, no. 10, pp. 489–497, 2010.

[31] J. Li, *The Study on Energy Dissipation and River Diversion Effect on Water Flow from Roughness Section on Carved Spillway, [M.S. Thesis]*, Xinjiang Agricultural University, Urumqi, China, 2016.

[32] F. Fan, Z. Mu, H. Zhang, and F. Li, "Experimental research on energy dissipation rate of rough strip energy dissipator in spillway bend," *Journal of Yangtze River Scientific Research Institute*, vol. 38, no. 12, p. 7, 2021.